Efficient Simulation of a Dynamic System with LuGre Friction

Nguyen B. Do

Aldo A. Ferri

School of Mechanical Engineering,
Georgia Institute of Technology,
Atlanta, GA 30332-0405

Olivier A. Bauchau
School of Aerospace Engineering,
Georgia Institute of Technology,
Atlanta, GA 30332-015

Friction is a difficult phenomenon to model and simulate. One promising friction model is the LuGre model, which captures key frictional behavior from experiments and from other friction models. While displaying many modeling advantages, the LuGre model of friction can result in numerically stiff system dynamics. In particular, the LuGre friction model exhibits very slow dynamics during periods of sticking and very fast dynamics during periods of slip. This paper investigates the best simulation strategies for application to dynamic systems with LuGre friction. Several simulation strategies are applied including the explicit Runge–Kutta, implicit Trapezoidal, and implicit Radau-IIA schemes. It was found that both the Runge–Kutta and Radau-IIA methods performed well in simulating the system. The Runge–Kutta method had better accuracy, but the Radau-IIA method required less integration steps. [DOI: 10.1115/1.2754304]

1 Introduction

Friction is a natural phenomenon that occurs in many engineering systems. In cases where the effects of friction cannot be ignored, a good friction model is necessary for the design, control, and analysis of the system. Although the concept of friction is easily understood, it is notoriously difficult to model and simulate. Many friction models contain a variety of nonlinear features such as discontinuities, hysteresis, internal dynamics, and other complications. These properties cause the friction models to be numerically stiff and therefore computationally cumbersome. For that reason, it would be advantageous to efficiently simulate a model that captures key characteristics of friction. In this paper, we will first present a brief summary of some classical friction models together with the LuGre friction model. Second, a simple dynamic model is presented to analyze the characteristics of the LuGre friction model. Next, the governing equations of the LuGre model are analyzed and the dynamic system is simulated using several numerical integration techniques. Finally, conclusions are made concerning the most efficient technique to simulate the LuGre friction model.

Numerical difficulties associated with simulation of frictional systems are well documented. See, for example, Armstrong-Hélouvry et al. [1] and Mitiguy and Banerjee [2]. The basic problem is one of numerical stiffness. Simple models of friction, derived from the Coulomb friction paradigm, suggest that the friction force changes "discontinuously" as the direction of interfacial slip changes. Figure 1 shows some typical sketches of friction force versus slip velocity. It should be noted that "sticking" of the frictional interface is characterized by zero slip velocity; therefore, it is not uncommon for the frictional interface to spend intermittent and finite periods of time at zero slip velocity, where the friction law is discontinuous.

If one starts from the assumption that the friction laws depicted in Fig. 1 properly reflect the behavior of sliding friction, the discontinuity presents a host of analytical and computational challenges. Simulation of the time response requires very fine time steps to maintain accuracy in regions where the slip velocity changes sign or where sticking occurs. Depending on the time-integration method used, it is even possible for numerical instabilities to develop. Two main strategies have been employed to deal with this problem. First, numerous studies have sought to "smooth" or "regularize" the friction law in the vicinity of the discontinuity. For example, the signum type nonlinearity depicted in Fig. 1(*a*), can be replaced with a saturation-type nonlinearity, as in Fig. 2, or a smoothly transitioning approximation as shown in Fig. 3. In both cases, the infinite slope at $v=0$ is replaced with a slope of order $1/\epsilon$, where ϵ is small relative to some characteristic slip velocity for the problem in question. Obviously, as $\epsilon \to 0$, the numerical stiffness of the problem becomes worse and worse. Consequently, time simulation of friction-damped systems that experience finite periods of sticking are burdened with very small time steps, necessitating high computation times in order to maintain stability and/or accuracy.

A second approach to address simulation of systems with discontinuous friction is to utilize a "switching strategy," also known as an event-driven strategy [3]. In this approach, the system is simulated either using the discontinuous friction law, or using a smoothed version thereof. However, when the slip velocity changes sign, one checks to determine whether the maximum-available friction force is sufficient to prevent slip from occurring. See, for example, Ferri and Heck [4] and Whiteman and Ferri [5]. Depending on the outcome of this check, one either continues to integrate the "slipping equations," or one switches to the use of "sticking equations," which model the system with a stuck interface. Variations of this idea have also appeared in the literature [4,6]. While this strategy alleviates the numerical stiffness problems associated with smoothing the discontinuity, it replaces it with another problem. As seen in Fig. 4, the accuracy of the method hinges on accurate determination of the switching time. The figure shows a transition from slipping to sticking, followed by renewed slip in the opposite direction. Due to errors in the computational solution, this switching time could be "delayed" (or "advanced") by some small amount of time. Equivalently, delays could occur due to the discrete nature of the numerical solution.

Of course, in reality, the physical friction process is not discontinuous. Various models of friction have been proposed that address this shortcoming by refining the behavior of the interface when the slipping velocity is small or when it changes sign. For example, "microslip" models allow small amounts of displacement to occur during "sticking." The most common microslip model is the Iwan model [7,8], also termed the elastic-perfectly plastic model [9]. In its simplest form, the model can be thought of as a spring in series with a Coulomb friction element having friction force μN. When the force in the spring reaches a magnitude of μN, the force in the Iwan model saturates until the direction of slip reverses. More complicated microslip behavior can be modeled if a number of spring-damper elements are placed in

Contributed by the Design Engineering Division of ASME for publication in the JOURNAL OF COMPUTATIONAL AND NONLINEAR DYNAMICS. Manuscript received September 1, 2005; final manuscript received March 18, 2007. Review conducted by Harry Dankowicz. Paper presented at the ASME 2005 Design Engineering Technical Conferences and Computers and Information in Engineering Conference (DETC2005), Long Beach, CA, USA, September 24–28, 2005.

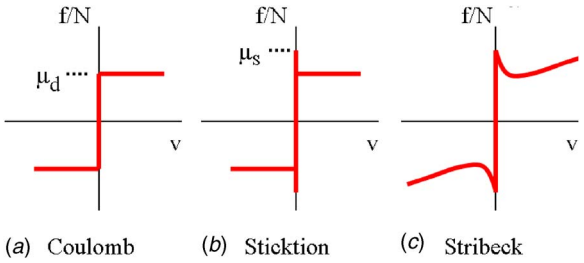

Fig. 1 Normalized friction force versus slip velocity: (*a*) Coulomb; (*b*) Sticktion; and (*c*) Stribeck friction laws

series or parallel; see, for example Sanliturk and Ewins [10], or Quinn and Segalman [11]. While conceptually simple, the algorithms necessary to implement Iwan models are surprisingly complicated [12]. The reason is that one must keep track of which friction elements have slipped and which have not. Iwan models also suffer from an inability to capture differing static and kinetic friction coefficients, which is an important attribute in stick-slip motion.

Another class of friction laws that capture the microslip and macroslip regimes in a single model may be termed *state-variable friction models* [1]. These models use additional states and associated differential equations to describe the friction force. Because of the internal dynamics of the friction model, the forces exhibit a hysteretic relationship to the gross interfacial displacement and/or velocity. Examples of friction models having internal dynamics include the Dahl model [13], the Valanis model [14,15], the LuGre friction model [16], and the Leuven model [17,18]. *Bristle models*

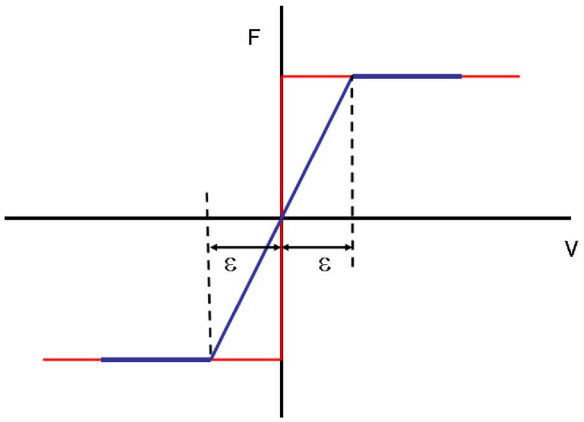

Fig. 2 Saturation approximation of signum nonlinearity

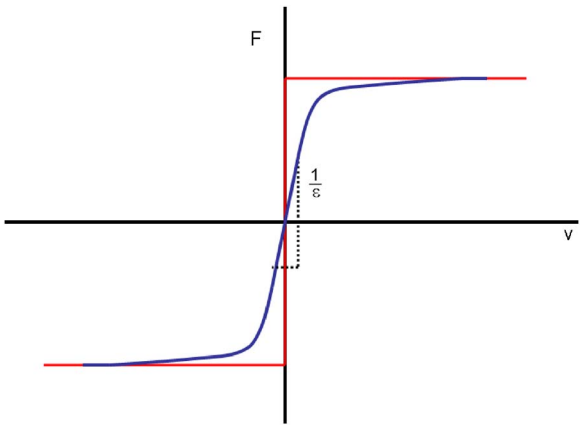

Fig. 3 Smooth approximation of signum nonlinearity

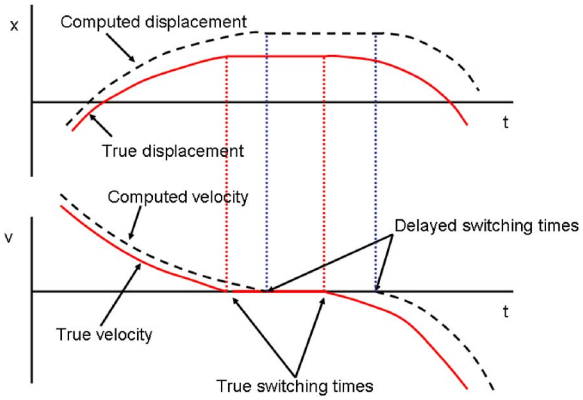

Fig. 4 Delayed switching time

have also been proposed that represent the friction interface as a collection of compliant bristles as depicted in Fig. 5. Microslip is captured by the bending of bristles prior to slip. Haessig and Friedland [19] proposed a model in which each bristle is treated individually, separating as bonds are broken, and then readhering. The LuGre friction model, so named because it was developed jointly by researchers at the Lund Institute of Technology, Sweden and the University of Grenoble, France, is also based on a bristle interpretation of the frictional interface, but it treats the collection of bristles in an aggregate fashion. The details of this model are the focus of this paper and are presented below.

2 LuGre Model

As discussed above, the LuGre model has become popular because it incorporates many of the observed features of frictional behavior. For example, imbedded within the LuGre model is the Stribeck effect, displayed in Fig. 1(*c*). The Stribeck model exhibits a negative derivative with respect to slip velocity, for small levels of slip velocity. This is one of the key features of friction that contributes to limit-cycle behavior and stick-slip oscillations in frictional systems. Furthermore, the LuGre model behaves like a linear spring/damper pair when it is linearized for small motions.

As mentioned above, the basis of the LuGre model is shown in Fig. 5. At the microscopic level, two surfaces make contact at various asperities. These asperities are represented with bristles, and the bristles deflect like a spring when there is a relative velocity between the two surfaces. The deflection of the springs gives rise to the friction force. If the deflection is sufficiently large, then the bristles will slip in a highly random manner because of the irregular surfaces. Although the deflection of the bristles is random, the LuGre model only considers the average deflection. The average deflection of the bristles, Z, is modeled by the first-order differential equation

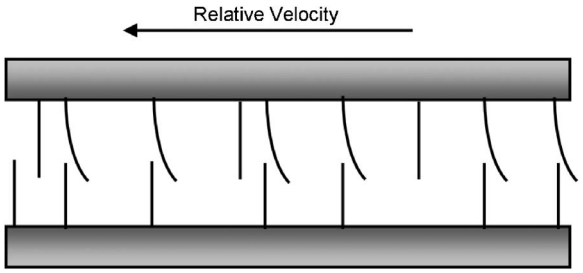

Fig. 5 Description of the frictional interface in the LuGre model

Table 1 LuGre friction model parameters [16]

Parameter	Value	Unit
σ_0	10^5	N/m
σ_1	$\sqrt{10^5}$	Ns/m
σ_2	0.4	Ns/m
F_c	1	N
F_s	1.5	N
V_s	0.001	m/s

$$\dot{Z} = V - \frac{|V|}{G(V)}Z \tag{1}$$

where V is the relative velocity between the two surfaces. The function $G(V)$ allows the LuGre model to accommodate a higher static coefficient of friction than dynamic coefficient of friction. One possible form for $G(V)$ was proposed in Canudas de Wit et al. [16]

$$G(V) = \frac{1}{\sigma_0}\{F_C + (F_S - F_C)e^{-(V/V_S)^2}\} \tag{2}$$

where F_C is the kinetic friction force; F_S is the static friction force; σ_0 is the aggregate bristle stiffness; and V_S is the Stribeck velocity. Roughly speaking, "sticking" is associated with the approximate velocity range $-V_S < V < V_S$. Finally, the LuGre friction force is given by

$$F_L(V,Z) = \sigma_0 Z + \sigma_1 \dot{Z} + \sigma_2 V \tag{3}$$

where σ_1 is a damping coefficient and σ_2 accounts for viscous friction. For this study, the values used for the LuGre parameters are listed in Table 1. Note that V_S is a very small slip velocity, below which the frictional interface can be thought of as being "stuck" or undergoing microslip.

3 System Modeling

To analyze the characteristics of the LuGre model, a simple mechanical system proposed by Canudas de Wit et al. [16] is used to focus the present discussion. The system, shown in Fig. 6, represents a mass, M, connected to a spring K that is being pulled by a constant velocity, $\dot{U}=R$. As the mass slides along, the LuGre friction force, $F_L(V,Z)$, acts between the ground and the mass. The position of the mass is denoted by X and its velocity is V. Two first-order equations govern the motion of the mass

$$\dot{X} = V \tag{4}$$

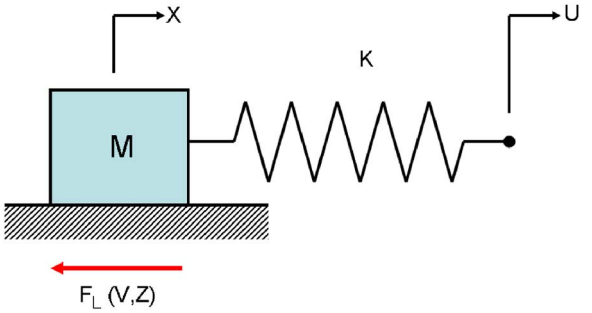

Fig. 6 Stick-slip system. The parameters are M=1 kg, K =2 N/m, and U increases at the constant rate of 0.1 m/s; i.e., U=0.1t m.

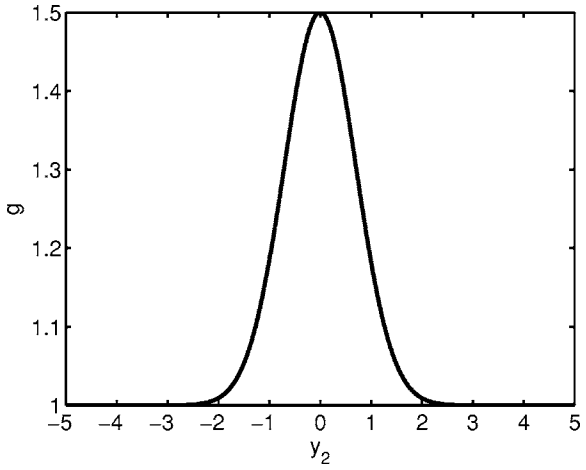

Fig. 7 LuGre function g versus y_2 using values in Table 1

$$\dot{V} = (KU - KX - F_L(V,Z))/M \tag{5}$$

It is useful to nondimensionalize the equations governing the mass as well as that of the LuGre force by introducing the following terms

$$y_1 = \frac{KX}{F_C}, \quad y_2 = \frac{V}{V_S}, \quad y_3 = \frac{\sigma_0 Z}{F_C}, \quad u = \frac{KU}{F_C}, \quad \omega_n = \sqrt{K/M}, \tag{6a}$$

$$\tau = \omega_n t$$

$$\alpha = \frac{KV_S}{\omega_n F_C}, \quad \gamma = \frac{F_S - F_C}{F_C}, \quad \epsilon = K/\sigma_0, \quad s_1 = \frac{\sigma_1 V_S}{F_C}, \quad s_2 = \frac{\sigma_2 V_S}{F_C} \tag{6b}$$

When Eq. (6) is introduced into Eqs. (4), (5), and (1), the following three equations are obtained

$$y_1' = \alpha y_2 \tag{7}$$

$$y_2' = (u - y_1 - f_L(y_2, y_3))/\alpha \tag{8}$$

$$\epsilon y_3' = \alpha y_2 - \alpha \frac{|y_2|}{g(y_2)} y_3 \tag{9}$$

where $'$ denotes a derivative with respect to nondimensional time, τ, and

$$f_L(y_2,y_3) = y_3 + s_1\left(y_2 - \frac{|y_2|}{g(y_2)}y_3\right) + s_2 y_2 \tag{10}$$

$$g(y_2) = 1 + \gamma \exp(-y_2^2) \tag{11}$$

It should be noted that other nondimensionalization schemes are possible. In particular, normalizing the velocity V by the characteristic speed $V_c = F_C\omega_n/K$ eliminates α in Eqs. (7)–(9), but introduces an additional α factor in the exponential term of g. As shown below, it is convenient to have a unity value of y_2 correspond to the Stribeck velocity.

Equations (7)–(9) can be conveniently represented in state-space form

$$y' = f(y,u) \tag{12}$$

where y is the state vector $[y_1\ y_2\ y_3]^T$ and $f(y,u)=[f_1\ f_2\ f_3]^T$ is formed from the right-hand sides of Eqs. (7)–(9), with ϵ moved to the right-hand-side of Eq. (9).

For the functional form investigated here, g dies out rapidly with y_2, as shown in Fig. 7; g is approximately equal to 1 for

$|y_2|>3$. Also note that the slope of g is zero at $y_2=0$, and is approximately zero outside the range $|y_2|>3$. The magnitude of the slope is maximum at $y_2=\pm 1/\sqrt{2}$, implying that the dynamics can change rapidly when the velocity is in the "sticking range," defined to be $|y_2|<1$.

It may be noted that Eqs. (7)–(9) are in standard, singular perturbation form [20]. The stiffness ratio $\epsilon=K/\sigma_0$ (not to be confused with ϵ in Figs. 2 and 3) is typically small, due to the relatively high bristle stiffness. Using the numerical values of Table 1, ϵ is equal to 2×10^{-5}. The smallness of the parameter ϵ is partially to blame for the "numerical stiffness" of the system of equations. Numerical stiffness makes it difficult to simulate the response of the system, because it necessitates very small time steps to ensure algorithm stability and accuracy. The problem is compounded when the system in question is more realistic, such as a multi-degree-of-freedom structure with multiple frictional interfaces. As the present system is only single-degree-of-freedom, it is possible to study the numerical stiffness problem analytically.

In order to examine the numerical stiffness of the LuGre dynamics, one can examine the Jacobian of the state dynamics

$$J=\begin{bmatrix} \frac{\partial f_1}{\partial y_1} & \frac{\partial f_1}{\partial y_2} & \frac{\partial f_1}{\partial y_3} \\ \frac{\partial f_2}{\partial y_1} & \frac{\partial f_2}{\partial y_2} & \frac{\partial f_2}{\partial y_3} \\ \frac{\partial f_3}{\partial y_1} & \frac{\partial f_3}{\partial y_2} & \frac{\partial f_3}{\partial y_3} \end{bmatrix} = A + B(y_2,y_3) + C(y_2) \tag{13}$$

where

$$A=\begin{bmatrix} 0 & \alpha & 0 \\ -1/\alpha & -(s_1+s_2)/\alpha & -1/\alpha \\ 0 & \alpha/\epsilon & 0 \end{bmatrix} \tag{14}$$

$$B(y_2,y_3)=\begin{bmatrix} 0 & 0 & 0 \\ 0 & s_1 y_3/\alpha & 0 \\ 0 & -\alpha y_3/\epsilon & 0 \end{bmatrix} \left\{ \frac{g+2\gamma y_2^2 \exp(-y_2^2)}{g^2} \right\} \mathrm{Sgn}(y_2) \tag{15}$$

and

$$C(y_2)=\begin{bmatrix} 0 & 0 & 0 \\ 0 & 0 & s_1/\alpha \\ 0 & 0 & -\alpha/\epsilon \end{bmatrix} \left\{ \frac{|y_2|}{g} \right\} \tag{16}$$

As it describes the "local dynamics" of the system, the Jacobian is useful in analyzing the source of the numerical stiffness when Eq. (12) is time integrated. In the case of explicit numerical integration routines, the stability of the algorithm depends on the size of the nondimensional time step, h. The maximum allowable time step is inversely proportional to the largest magnitude eigenvalue of J. As seen above, the matrix A has no dependence on the state vector y. For sufficiently large $|y_2|$, the matrix B becomes independent of y_2, except for a dependence on the sign of y_2. The matrix C, however, grows linearly with $|y_2|$, dominating matrices A and B for high slip velocities ($|y_2|\gg 10$). Thus, an expression for the largest magnitude eigenvalue of J that holds asymptotically as $|y_2|$ gets larger and larger can be derived based on the nonzero eigenvalue of C

$$\lambda_{\max}(J)=\frac{\alpha|y_2|}{\epsilon g} \tag{17}$$

It is seen that $\lambda_{\max}$ grows linearly with $|y_2|$. Therefore, as the velocity of the mass becomes large compared to the Stribeck velocity, V_S, the maximum allowable time step becomes smaller. It is also seen that $\lambda_{\max}$ is inversely proportional to $\epsilon=K/\sigma_0$. Thus as the aggregate bristle stiffness σ_0 grows larger, the numerical stiffness problem worsens, especially during episodes of high slip velocity. In dimensional terms, $\lambda_{\max}(J)=V\sigma_0/F_C\ \mathrm{s}^{-1}$.

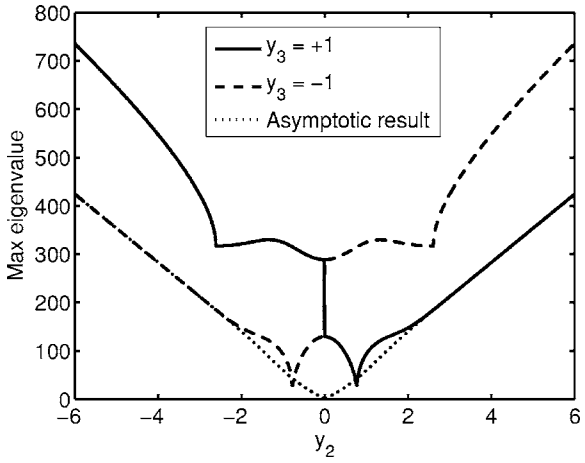

Fig. 8 Maximum magnitude eigenvalue versus y_2

An alternate interpretation of Eq. (17) is obtained by inspection of the LuGre dynamics Eq. (9). If, over a small interval, the nondimensionalized velocity (y_2) is assumed to be constant, then the coefficients of Eq. (9) are constant over this interval. Subsequently, Eq. (9) becomes a linear first-order differential equation with a time constant, T_c

$$y_3'=\frac{\alpha}{\epsilon}y_2-\frac{\alpha}{\epsilon}\frac{|y_2|}{g(y_2)}y_3=\frac{\alpha}{\epsilon}y_2-\frac{y_3}{T_c} \tag{18}$$

where

$$T_c=\frac{\epsilon g}{\alpha|y_2|} \tag{19}$$

From Eq. (19), it is evident that the time constant is equal to the inverse of the maximum eigenvalue given by Eq. (17). For very low values of y_2, the time constant is very large, indicating very slow friction dynamics. As the velocity emerges from the sticking range, $|y_2|\approx 1$, g falls off rapidly, decreasing the time constant. For $|y_2|>3$, $g(y_2)$ is approximately 1 and T_c decreases inversely with y_2. As the time constant tends to zero, the dynamics of the friction model are much faster than that of the mechanical system. Qualitatively, this behavior can be attributed to the movement of the bristles. During microslip, the bristles move in a slow, linear manner. When the critical limit is reached, the bristles "snap" back to place and cause an increase in the speed of the friction dynamics. As the velocity increases, the frequency of contact between the bristles increases, therefore causing the bristles to move faster. The difference between the speed of the friction dynamics and that of the mass-spring system is what leads to numerical stiffness. This difference results in the requirement of small time steps and the associated long computation times.

During sticking, which corresponds to zero values of both y_2 and y_3, the eigenvalues of J are given by A alone. By inspection, one eigenvalue of A is identically zero. Using the friction parameters of Table 1, with $K=2$ N/m and $M=1$ kg, it is found that $\alpha=1.414\times 10^{-3}$, $\gamma=0.5$, $\epsilon=2\times 10^{-5}$, $s_1=0.3162$, and $s_2=4\times 10^{-4}$. With these nondimensional parameters values, the remaining two eigenvalues are calculated to be $-111.94\pm 193.57i$, which correspond to a magnitude of $\lambda_{\max}(J)=223.61$ and a damping ratio of 0.50. For small-to-moderate values of y_2, one must compute $\lambda_{\max}(J)$ numerically. Due to the presence of the matrix B, $\lambda_{\max}$ is a function of both y_2 and y_3. Also note that B captures the sensitivity of the Jacobian to the high slope of the function g within the range $|y_2|<1$. Figure 8 shows $\lambda_{\max}(J)$ versus y_2 for $y_3=\pm 1$. Also shown is the asymptotic expression for $\lambda_{\max}(J)$ given by Eq. (17).

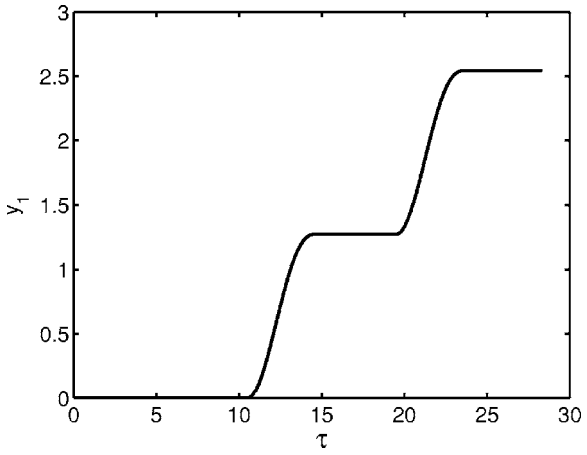

Fig. 9 y_1 versus τ using *ode45* with RelTol=1×10^{-4} and AbsTol=1×10^{-6}

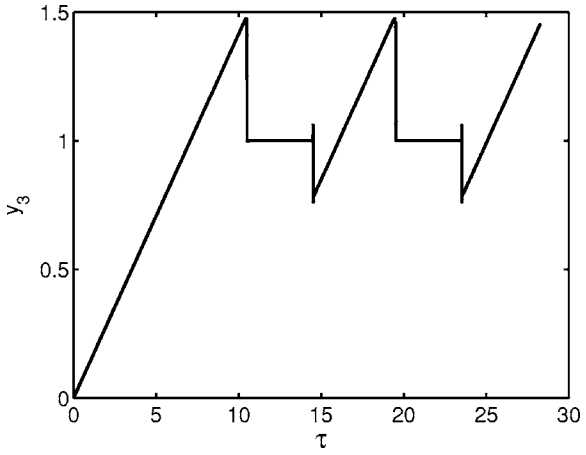

Fig. 11 y_3 versus τ using *ode45* with RelTol=1×10^{-4} and AbsTol=1×10^{-6}

For small velocities, the bristle displacement y_3 produces a difference in the maximum eigenvalue from the asymptotic result. However, as $|y_2|$ increases, this difference becomes less and less significant when viewed as a percent of $\lambda_{max}(J)$.

A number of conclusions can be drawn from Fig. 8. It is seen that the system is relatively well conditioned for low velocities ($|y_2|<3$), including the microslip region. The system becomes more and more ill conditioned as the slip velocity grows. This is in stark contrast to the regularization schemes portrayed in Figs. 2 and 3. When the discontinuity is smoothed in the vicinity of the zero-slip point, the system of equations is ill conditioned for small velocities (microslip) and becomes better conditioned as the slip velocity increases in magnitude.

This contrast may appear at first to be counterintuitive, because it is at odds with the behavior of standard approaches of friction modeling and simulation discussed in Sec. 1. Whether one smoothes the discontinuity or uses switching between sticking and slipping dynamical systems, the numerical problems are all located in the vicinity of *small slip velocities*. In the LuGre model of friction, sticking and near-sticking conditions are where the system is *relatively well conditioned*; ill conditioning develops as the slipping velocity gets larger.

4 Numerical Simulation Results

To initially simulate the stick-slip system, the MATLAB function *ode45* was used. The *ode45* function is based on an explicit Runge–Kutta formula, the Dormand–Prince pair [21,22]. The routine uses a variable time step, based on specified tolerances: a relative tolerance, RelTol, whose default value is 1×10^{-3}, and an absolute tolerance, AbsTol, whose default value is 1×10^{-6}. Figures 9–11 show the nondimensional state quantities while Fig. 12 shows the nondimensional LuGre friction force, $f_L(y_2,y_3)$. In the case shown, RelTol=1×10^{-4}, and AbsTol=1×10^{-6}. Note that the friction force behaves irregularly during the stick-slip regions. This irregular behavior can be attributed to the sudden change from the static friction force to the kinetic friction force. Further examination shows that at the instant the system begins to slip, the friction force initially decreases before increasing with increasing velocity. This phenomenon is consistent with the Stribeck effect. Finally, like the elastic friction model, the friction force during the sticking phase acts like a linear spring.

From Figs. 9 and 10, the displacement and velocity are fairly smooth and accurate, with results closely matching scaled results from Canudas de Wit et al. [16]. The LuGre force, on the other hand, exhibits a noticeable "ringing" in time intervals of high slip velocity. The ringing largely disappears when RelTol and AbsTol are lowered to 1×10^{-8}.

The reason for the ringing in the friction force is uncovered by examining the Jacobian at each point along the state trajectory. Figure 13 shows $\lambda_{max}(J)$ versus τ from a more accurate simulation using *ode45* with RelTol=1×10^{-7} and AbsTol=1×10^{-7}. It is seen that the time intervals in which the largest eigenvalue mag-

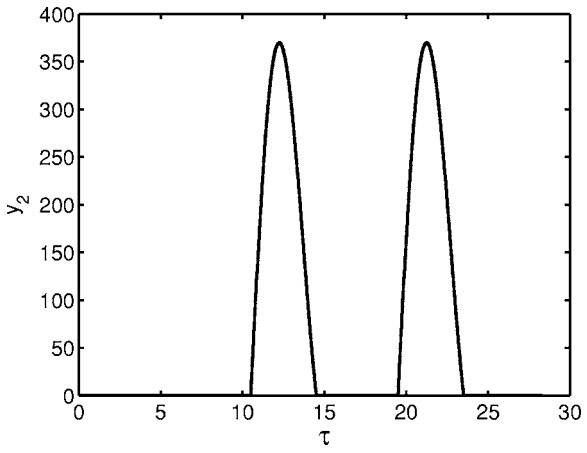

Fig. 10 y_2 versus τ using *ode45* with RelTol=1×10^{-4} and AbsTol=1×10^{-6}

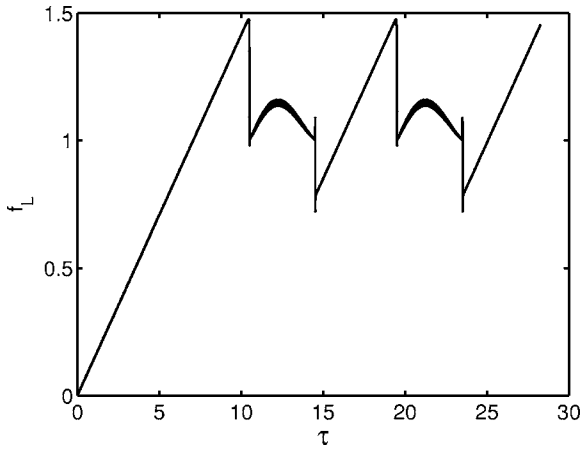

Fig. 12 f_L versus τ using *ode45* with RelTol=1×10^{-4} and AbsTol=1×10^{-6}

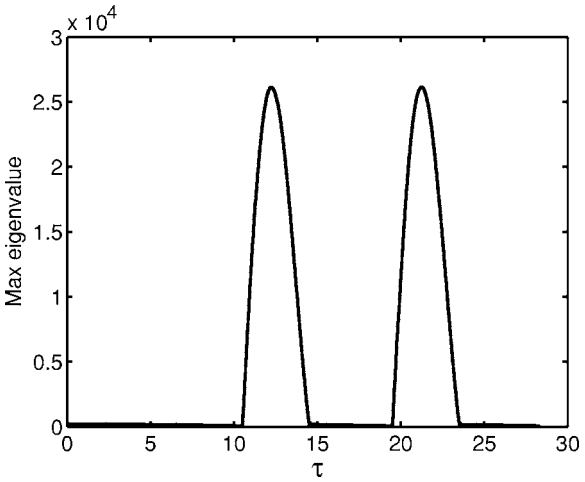

Fig. 13 $\lambda_{max}(J)$ **versus** τ**; from** *ode45* **with RelTol=1×10^{-7} and AbsTol=1×10^{-7}**

nitudes occur are closely related to occurrences of high slip velocities. Figure 14(*a*) shows a closeup of $\lambda_{max}(J)$ just as the mass transitions from microslip to macroslip, and Fig. 14(*b*) shows $\lambda_{max}(J)$ just after the first interval of macroslip comes to an end. For comparison, the figures also show the asymptotic result calculated by Eq. (17).

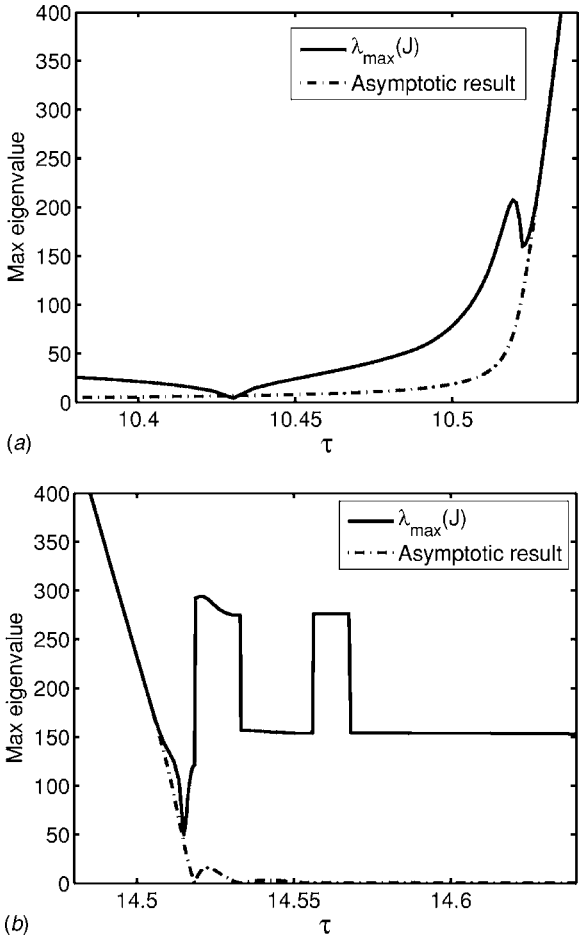

Fig. 14 (***a***) **Maximum eigenvalue during the transition from microslip to macroslip; and** (***b***) **maximum eigenvalue during the transition from macroslip to microslip**

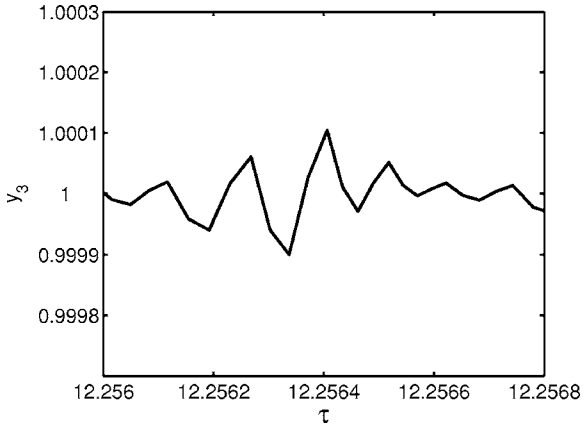

Fig. 15 Closeup of y_3 **versus** τ**;** *ode45* **with RelTol=1×10^{-4} and AbsTol=1×10^{-6}**

The large size of $\lambda_{max}(J)$ during periods of high slip velocity is the major source of the ringing that is evident in the LuGre friction force. However, the ringing that is present in the state vector itself is far less pronounced. In fact, only the bristle displacement y_3 displays any appreciable ringing during high slip rates. Figure 15 shows a closeup of y_3 during the period of maximum slip. It is seen that the ringing in y_3 amounts to approximately 0.01% of the nominal value. The ringing is amplified in the LuGre force because of the way that f_L is calculated; in particular, the expression in parentheses in Eq. (11) involves the subtraction of two terms that are large, and almost exactly equal. Operations of this type are prone to round off errors during computation.

It must be mentioned that the nondimensionalization of the terms associated with the LuGre friction model is very important for time simulation. Due to the size of the bristle stiffness, the dimensional displacement Z is orders of magnitude smaller than X and V. Consequently, direct integration of the dimensional system of equations is less accurate due to roundoff errors.

5 Comparison of Integration Methods

To find the best strategies to simulate the stick-slip system, several techniques were considered. Aside from using built-in MATLAB functions, the techniques included user-defined explicit and implicit time integration methods. The main difference between explicit and implicit integration schemes is in the formulation. Explicit schemes use past states to define the current states, whereas implicit schemes define the current states using past and current results. Furthermore, one can guarantee the stability of the result using implicit methods. As a note, all computer simulations were done using MATLAB 6.1 on a Pentium 4, 2.4 GHz computer. Also, the simulation time interval was from 0 s to 20 s.

5.1 Explicit Integration Methods. Although the use of a MATLAB function was useful as a first attempt to solve the system, it was necessary to write a user-defined integration scheme to fully understand and control the simulation process. Because of its popularity and efficiency, the fourth-order Runge–Kutta method was chosen as the explicit solver. Like the *ode45* function, this Runge–Kutta method is an explicit, time-marching scheme with a time step, h, a local error on the order of h^5, and a global error on the order of h^4 [23]. Since the maximum allowable time step is proportional to the inverse of the largest magnitude eigenvalue of the Jacobian, a time step based on this value was used for the baseline simulation. From Eq. (17), $\lambda_{max}=2.62\times10^4$ for the maximum value of $|y_2|$ in the simulation, which corresponds to a minimum time constant of 3.82×10^{-5}. To best capture the dynamics of the system, a time step of 10^{-5} was used, which was more than three times less than the minimum time constant. Note that the

Table 2 Comparison of explicit methods

Simulation method	Time step	Error		Simulation time (%)	Number of steps
		Max	RMS		
Runge-Kutta (baseline)	10^{-5}	n/a[b]	n/a[b]	100	2.828×10^{6}
Runge-Kutta (time constant)	$(1/3)T_c$ or 10^{-3}	0.103	1.50×10^{-3}	14.8	4.020×10^{5}
Ode45[a]	n/a[b]	1.68×10^{-4}	1.89×10^{-7}	3.62	1.476×10^{5}
Runge-Kutta (velocity)	10^{-4} or 10^{-3}	0.320	5.71×10^{-3}	1.17	3.170×10^{4}
Runge-Kutta (constant)	10^{-3}	3.98×10^{-4}	5.17×10^{-6}	1.14	2.829×10^{4}

[a]Absolute tolerance=relative tolerance=10^{-8}.
[b]Not available.

time step used, h, is in nondimensional form defined by $h=\omega_n H$, where H is the dimensional time step.

Although the baseline simulation ($h=10^{-5}$) gave the best results, it was not necessary to use such a small time step at all times. From previous analyses, the dynamics of the system is fast during periods of slip, but slow during microslip. Hence, it would be advantageous to base the time step on the local dynamics of the system. One way to vary the time step was to define h based on the inverse of the maximum eigenvalue, as shown in Fig. 13. However, this would be cumbersome because finding the eigenvalues of the Jacobian at each time step would be computationally expensive. The added overhead for such a technique would be prohibitive, especially for realistic systems having a higher number of degrees of freedom.

Another way to estimate the time step necessary to simulate the system was to use the time constant, as defined by Eq. (19). From Figs. 14(*a*) and 14(*b*), the inverse of the time constant agrees well with the maximum eigenvalue during episodes of high slip. The periods where these values do not agree are the transitional periods and during sticking. However, this disagreement can be addressed by setting a maximum time constant such that the integration scheme remains stable. For the system under consideration here, this maximum time constant was set to 10^{-3}. Otherwise, the time step was given by $T_C/3$. In other words, $h=\min(1\times10^{-3}, T_C/3)$.

To make the simulation more efficient, another method based on the velocity was used to estimate the time step. Because the dynamics of the system change rapidly at the stick/stick transition periods, a small time step (10^{-4}) was used in this region. Otherwise, the time step was set to 10^{-3}. This stick/slip transition region was defined as the range $0.1\leqslant|y_2|<5$.

Table 2 compares the different explicit methods in order of decreasing simulation time. In addition to the baseline case (fourth order Runge–Kutta with $h=\text{constant}=10^{-5}$), four other cases are shown: fourth-order Runge–Kutta with h switched based on the time constant, ode45 with RelTol=AbsTol=10^{-8}, fourth-order Runge–Kutta with h switched based on $|y_2|$, and fourth-order Runge–Kutta with $h=\text{constant}=10^{-3}$. Two different error metrics were employed. First, the error, E, was computed by taking the absolute value of the difference in the nondimensional friction forces at each instant in time. The first error metric listed in Table 2 is simply the maximum of E over the duration of the simulation. The second error metric is the root-mean-squared error, E_{RMS}, given by

$$E_{\text{RMS}}=\sqrt{\frac{1}{T}\int_0^T E^2\,d\tau} \tag{20}$$

where T is the final nondimensional time. Since the number of time steps was different for each method, the data were interpolated from the baseline data set for comparison. Finally, the simulation time is reported as a percentage to the baseline simulation time, which is 1651 s, or 27.5 min.

Table 2 shows that there is a significant improvement in the simulation time by switching the time step based on the time constant of the system. However, the maximum error using this method is unacceptable (~14% error) and the number of steps required is still relatively large. The Runge–Kutta method with h switching based on the velocity performed much better in terms of simulation time and number of steps, but its accuracy was the worst. The result using *ode45* had the best accuracy and a very short simulation time compared to the baseline. Finally, using the Runge–Kutta method with a constant time step of 10^{-3} produced errors comparable to the *ode45* method, but with the smallest simulation time and least amount of steps. This last result is surprising since 10^{-3} is roughly 26 times larger than the frictional time constant at the point of maximum slip velocity.

5.2 Implicit Integration Methods. Despite moderate successes with the explicit methods, implicit integration schemes were used to simulate the stick-slip system. The key advantage of the implicit integration methods is better stability characteristics versus the explicit methods. Therefore, it would be possible to use larger time steps (than the explicit methods) to simulate the LuGre model, even during slip. However, the disadvantage of implicit methods is the need to iterate at each time step. This iteration is necessary to solve for simultaneous equations at each time instant. Finally, despite the improved stability characteristics, the accuracy of the implicit methods still depends upon the size of the time step.

The first implicit method to be applied to the stick-slip system was the trapezoidal method. This technique is effective for solving stiff differential equations [23]. An extension of the trapezoidal method is the Radau-IIA method [24,25]. Both the trapezoidal integration scheme and the Radau-IIA scheme can be expressed in a common framework. At each time t_i, two sets of nonlinear equations must be solved for the unknown vectors, k_1 and k_2

$$k_1=f(y(t_i)+c_1k_1+c_2k_2, u(t_i+b_1)) \tag{21}$$

$$k_2=f(y(t_i)+c_3k_1+c_4k_2, u(t_i+h)) \tag{22}$$

where k_1 and k_2 are 3×1 vectors that approximate in some sense the average dynamics over a time step. The value of the state vector at the next time step is expressed in terms of k_1 and k_2 as follows

$$y(t_i+h)=y(t_i)+c_3k_1+c_4k_2 \tag{23}$$

For trapezoidal integration

$$c_1=c_2=0,\quad c_3=c_4=h/2,\quad b_1=0 \tag{24}$$

For Radau-IIA

Table 3 Comparison of implicit methods

Simulation method	Time step	Error (N) Max	Error (N) RMS	Simulation time (%)	Number of steps
Runge–Kutta (baseline)	10^{-5}	n/a[a]	n/a[a]	100	2.828×10^{6}
Trapezoidal	5×10^{-3}	0.150	3.37×10^{-3}	2.25	5.658×10^{3}
Radau-IIA (constant)	10^{-2}	9.33×10^{-2}	2.11×10^{-3}	1.08	2.830×10^{3}
Radau-IIA (velocity)	10^{-2} or 0.02	0.497	2.63×10^{-2}	0.56	1.436×10^{3}
Radau-IIA (time constant)	10^{-2} or 0.05	0.490	3.24×10^{-2}	0.47	1.216×10^{3}

[a]Not available.

$$c_1 = 5h/12, \quad c_2 = -h/12, \quad c_3 = 3h/4, \quad c_4 = h/4, \quad b_1 = h/3 \tag{25}$$

As for the explicit methods, various schemes were investigated for their accuracy and efficiency. The results of the implicit integration methods are summarized in Table 3. The trapezoidal method was implemented with a constant time step of $h=0.005$. The Radau-IIA method was compared using three different schemes for selection of h: $h=\text{constant}=10^{-2}$, h switched based on velocity, and h switched based on the time constant. In the velocity-switching case, $h=0.01$ if $0.1<|y_2|<5$, and $h=0.02$ otherwise. In the time-constant-switching case, $h=0.01$ when $T_C<0.1$, and $h=0.05$, otherwise.

When compared to the explicit methods in Table 2, the implicit methods on average require less time and much fewer integration steps. The primary reason for these improvements is that larger time steps (than the explicit methods) could be used to obtain an accurate solution. Although the equations of the LuGre model are numerically stiff, the implicit integration schemes are well suited to solve them.

Similar to the findings for the Runge–Kutta method, it is observed that the maximum error values for the variable time step methods were unacceptably large. A reason for the relatively large errors was that at the stick/slip transition regions, there was a shift in the solution compared to the baseline. This shift occurred for both the explicit and implicit methods that used a variable time step. Since the transitions in the friction force occur very rapidly in time, even a small time shift in one simulation relative to the baseline result can give rise to very large maximum errors.

From Tables 2 and 3, it appears that the best choice to simulate the stick-slip system is to use the Radau-IIA method with a constant time step of 10^{-2}. Surprisingly, the use of fourth-order Runge–Kutta with a constant time step of 10^{-3} also displayed a good balance between accuracy and efficiency. In terms of simulation time, both the fourth-order Runge–Kutta and Radau-IIA methods are similar. The Runge–Kutta method has errors two orders of magnitude better than the Radau-IIA scheme, however, the Radau-IIA requires an order of magnitude fewer steps. Thus the best choice of integration scheme may depend on the users' preference for accuracy versus speed, as well as on the availability of computer memory.

6 Conclusions

The purpose of this study was to efficiently simulate a dynamic system having LuGre friction. The LuGre friction model was chosen because it incorporated many characteristics of other friction models. To analyze the behavior of the LuGre model, a second-degree-of-freedom (SDOF) spring-mass system sliding against a fixed surface was considered. The equations of motion for this system were converted to a nondimensional form for convenience as well as to prevent roundoff errors in the calculations. The spring-mass system was analyzed by observing the linearized dynamics of the entire system as well as the time constant of the LuGre model alone. The analysis shows that the friction dynamics can be very fast and therefore numerically stiff during periods of high slip rate. Furthermore, the dynamics change rapidly at stick-slip transitions. It is found that the system dynamics are relatively well conditioned during periods of sticking, which stands in contrast to the standard behavior of other friction models.

The SDOF system was simulated using explicit and implicit time integration methods. In general, the explicit methods required smaller time steps than the implicit methods. Consequently, this requirement led to longer simulation times as well as a larger number of integration steps. However, the explicit methods performed better in terms of accuracy. Attempts to reduce the simulation time by varying the time steps performed poorly for both explicit and implicit methods. This poor performance was attributed to a slight time shift in the solution, which caused relatively large errors. The best simulation methods were found to be the explicit Runge–Kutta and implicit Radau-IIA methods with constant time steps of 10^{-3} and 10^{-2}, respectively. Determining which is the best method depends on one's need for better accuracy (Runge–Kutta) or reduced memory usage (Radau-IIA). However, when simulating a large dynamical system, using a larger time step would greatly reduce the computation time. This advantage outweighs improved accuracy afforded by the Runge–Kutta method. Therefore, for large systems with LuGre friction, the Radau-IIA method is the best method for numerical integration.

Natural extensions of this study would be to apply the LuGre model to higher order systems with various types of boundary conditions and excitations. Ultimately, it is the goal of the authors to incorporate this friction model into multibody and finite element codes to solve large scale problems.

Acknowledgment

The authors would like to thank the Air Force Office of Scientific Research (AFOSR) for providing funding for this research, under Contract No. F49620-03-1-0176.

References

[1] Armstrong-Hélouvry, B., Dupont, P., and Canudas de Wit, C., 1994, "A Survey of Models, Analysis Tools and Compensation Methods for the Control of Machines with Friction," Automatica, **30**(7), pp. 1083–1138.
[2] Mitiguy, P. C., and Banerjee, A. K., 1999, "Efficient Simulations of Motion Involving Coulomb Friction," J. Guid. Control Dyn., **22**(1), pp. 78–86.
[3] Pfeiffer, F., and Glocker, C., 1996, *Multibody Dynamics with Unilateral Contact*, Wiley, New York, NY.
[4] Ferri, A. A., and Heck, B. S., 1997, "Analysis of Stick-Slip Motion in Coulomb Damped Systems Using Variable Structure System Theory," *Proceedings of the 1997 ASME Design and Technical Conferences*, Sacramento, CA, September 14–17.
[5] Whiteman, W. E., and Ferri, A. A., 1997, "Multi-Mode Analysis of Beam-Like Structures Subjected to Displacement-Dependent Dry Friction Damping," J. Sound Vib., **201**(3), pp. 403–418.
[6] Karnopp, D., 1985, "Computer Simulation of Stick-Slip Friction in Mechani-

cal Dynamic Systems," ASME J. Dyn. Syst., Meas., Control, **107**(1), pp. 100–103.
[7] Iwan, W. D., 1966, "A Distributed-Element Model for Hysteresis and Its Steady-State Dynamic Response," ASME J. Appl. Mech., **33**, pp. 893–900.
[8] Iwan, W. D., 1967, "On a Class of Models for the Yielding Behavior of Continuous and Composite Systems," ASME J. Appl. Mech., **34**, pp. 612–617.
[9] Ferri, A. A., 1995, "Friction Damping and Isolation Systems," ASME J. Vibr. Acoust., **117B**, pp. 196–206.
[10] Sanliturk, K. Y., and Ewins, D. J., 1996, "Modelling Two-Dimensional Friction Contact and Its Application Using Harmonic Balance Method," J. Sound Vib., **193**(2), pp. 511–523.
[11] Quinn, D. D., and Segalman, D. J., 2005, "Using Series-Series Iwan-Type Models for Understanding Joint Dynamics," ASME J. Appl. Mech., **72**(5), pp. 666–673.
[12] Song, Y., Hartwigsen, C. J., McFarland, D. M., Vakakis, A. F., and Bergman, L. A., 2004, "Simulation of Dynamics of Beam Structures With Bolted Joints Using Adjusted Iwan Beam Elements," J. Sound Vib., **273**, pp. 249–276.
[13] Dahl, P. R., 1976, "Solid Friction Damping of Mechanical Vibrations," AIAA J., **14**, 1675–1682.
[14] Gaul, L., and Nitsche, R., 2001, "The Role of Friction in Mechanical Joints," Appl. Mech. Rev., **54**(2), pp. 93–106.
[15] Valanis, K. C., 1971, "A Theory of Viscoplasticity Without a Yield Surface," Arch. Mech., **23**(4), pp. 171–191.
[16] Canudas de Wit, C., Olsson, H., Astrom, K. J., and Lischinsky, P., 1995, "A New Model for Control of Systems with Friction," IEEE Trans. Autom. Control, **40**(3), pp. 419–425.
[17] Swevers, J., Al-Bender, F., Ganesman, C. G., and Prajogo, T., 2000, "An Integrated Friction Model Structure with Improved Presliding Behavior for Accurate Friction Compensation," IEEE Trans. Autom. Control **45**(4), pp. 675–686.
[18] Lampaert, V., Swevers, J., and Al-Bender, F., 2002, "Modification of the Leuven Integrated Friction Model Structure," IEEE Trans. Autom. Control, **47**(4), pp. 683–687.
[19] Haessig, D. A., Jr., and Friedland, B., 1991, "On the Modeling and Simulation of Friction," ASME J. Dyn. Syst., Meas., Control, **113**, pp. 354–362.
[20] Kokotovic, P., Khalil, H., and O'Reilly, J., 1986, *Singular Perturbation Methods in Control: Analysis and Design*, Academic, London, UK.
[21] Forsythe, G., Malcolm, M., and Moler, C., 1977, *Computer Methods for Mathematical Computations*, Prentice-Hall, Englewood Cliffs, NJ.
[22] Kahaner, D., Moler, C., and Nash, S., 1989, *Numerical Methods and Software*, Prentice-Hall, Englewood Cliffs, NJ.
[23] Faires, J. D., and Burden, R., 1998, *Numerical Methods*, 2nd ed., Brooks/Cole Publishing Co., Pacific Grove, CA.
[24] Hairer, E., and Wanner, G., 1991, *Solving Ordinary Differential Equations II: Stiff and Differential-Algebraic Problems*, Springer-Verlag, Berlin, Germany.
[25] Hairer, E., and Wanner, G., 1999, "Stiff Differential Equations Solved by Radau Methods," J. Comput. Appl. Math., **111**, pp. 93–111.